Mesoscale Modeling of Chloride Penetration in Unsaturated Concrete Damaged by Freeze-Thaw Cycling

Licheng WANG[1] and Tamon Ueda[2]

Abstract: For concrete structures exposed to frost attack, cracks or microcracks induced by freeze-thaw cycling can format interconnecting flow paths and allow more water or chloride ions to penetrate into the bulk concrete. It will subsequently facilitate further deterioration of concrete structures and accelerate the corrosion of embedded reinforced steel bars. Moreover, in reality most concrete structures are rarely fully saturated, so that chloride transportation in unsaturated concrete must be studied with respect to the water moving process in order to cover the real existing service conditions. In the current work, a numerical simulation method based on the mesoscale composite structure of concrete, named the lattice network model, is established to analyze the penetration property of concrete; especially the effects of microcracking induced by freeze-thaw damage on the unsaturated flow behavior are investigated. In the mesoscale model, concrete is treated as a three-phase composite material consisting of coarse aggregates, mortar matrix and interfacial transition zone (ITZ) between the aggregate and the mortar matrix. The diffusivities of each phase, i.e., water and chloride diffusion coefficients, is separately characterized and quantified in terms of the published test results. The unsaturated flow theory for capillary water absorption and chloride transport is employed to simulate the ingress of water and chloride ions into concrete. It is found

[1]Associate Professor, State Key Laboratory of Coastal and Offshore Engineering, Dalian Univ. of Technology, No. 2, Linggong Road, Dalian 116024, China. E-mail: wanglicheng2000@163.com

[2]Professor, Division of Engineering and Policy for Sustainable Environment, Faculty of Engineering, Hokkaido Univ., Kita-ku, Kita 13, Nishi 8, Sapporo 060-8628, Japan.

that the water absorption and chloride penetration are substantially influenced by the frost action, and the cumulative absorbed water and chloride penetration depth are increased with the increase of freezing-thawing cycles (FTCs). Furthermore, the numerical predictions about water absorption and chloride profiles are compared with the experimental measurements. The comparisons indicate that numerical predictions agree very well with the test data.

CE Database subject headings: Concrete; Cracking; Freeze-thaw; Chlorides; Absorption

Author keywords: Chloride; unsaturated concrete; freezing-thawing cycles (FTCs); numerical modeling; mesoscale; lattice network model.

Introduction

Degradation of concrete structures has attracted more and more attention in recent years although concrete was once treated as a durable maintenance-free construction material. The deterioration mechanism of concrete facilities can be summarized as carbonation, sulfate and chloride attack, freezing-thawing cycles (FTCs), and so on. Generally, in the ingressive environment, penetration of chloride ions through concrete cover is a major factor affecting the durability of reinforced concrete structures because it can result in corrosion of the reinforcing bars (Boddy et al. 1999). Furthermore, the formation of rust in the interface between steel bars and surrounding concrete is associated with large volume expansion, which may cause cracking, spalling, and delamination of the concrete cover. Particularly in the severe rust cases, the bearing capacity of the structural members may be decreased due to the reduction of the cross-section of reinforcement (Ababneh et al. 2003). Therefore, there is growing interest in clarifying the deterioration mechanism and to predict the life-cycle performance of concrete structures.

In reality, most concrete structures are always subjected to cyclic drying-wetting actions by wind, sun, rain/snow fall and water level of ocean/river. Coastal and marine structures in splash and

tidal zones are a good example. Concrete within the splashing and tidal zones is not fully saturated. The process of chloride ingress in partially saturated concrete is clearly different from that in fully saturated concrete because of the different driving force and transport mechanism (Nagesh and Bhattacharjee 1998). There exist two transport mechanisms for chloride ions penetrating in the unsaturated concrete; one is the capillary suction of chloride-containing water into partially water-filled pores and the other is the diffusion of chloride ions in water-filled pores. It has been shown that the transport of chlorides by capillary suction makes greater contribution than by diffusion in the partially saturated concrete (Lunk 1998; Nagesh and Bhattacharjee 1998), since under this condition the diffusion is a quite slow process in comparison with the capillary suction. This has already been confirmed by some experimental findings. For example, Nielsen and Geiker (2003) concluded that chloride diffusion coefficient in saturated condition was about 5 times higher than that with RH of 65%. Climent et al. (2002) and de Vera et al. (2007) found that the diffusion coefficient decreased about two orders of magnitude, from 6×10^{-12} m^2/s to 2×10^{-14} m^2/s approximately, when the degree of water saturation was lowered from values of 0.7-0.8 to values of 0.3-0.4. The fact that corrosion of steel reinforcement in the splashing and tidal zone is most severe can be partly attributed to the alternate wetting and drying which result in high chloride and oxygen content. To properly describe the deterioration process of reinforced concrete structure under the unsaturated condition, the chloride ingress by capillary absorption must be taken into account.

In addition, water penetration depth significantly depends on the characteristics of porosity in the surface layer of concrete, including the pore diameter and distribution, and the pore continuity and tortuosity (McCarter et al. 1992; Kelham 1988). When subjected to freeze-thaw cycling, concrete deteriorates through a variety of physical and chemical process, which will result in cracking, and subsequently increase the porosity of concrete. It has been widely realized that the

66 existence of cracks in concrete can significantly modify the transport properties of the material
67 (Gérard et al. 1996; Wang et al. 1997; Aldea et al. 1999; Yang et al. 2006; Sahmaran et al. 2007).
68 Moreover, cracking due to freeze-thaw cycling generally forms interconnecting flow paths and
69 allows more water or chloride ions to penetrate into the concrete, thus facilitating further
70 deterioration. A number of studies have shown that increased chloride transport due to cracking can
71 accelerate the corrosion of reinforced steel in concrete (Schiessl and Raupach1997; Qi 2003; Jaffer
72 and Hansson 2008). Therefore, in a cold and ingressive environment, it is necessary to properly take
73 into account the internal cracking or damage of concrete caused by freeze-thaw cycling in order to
74 realistically estimate the reduction of bearing capacity of RC structural members and then to predict
75 their durability and life-cycle performance. The mechanical behavior of frost-damaged concrete has
76 been successfully simulated by means of a mesoscale numerical model (Ueda et al. 2009). However,
77 few works have been done to investigate the agents moving process and mechanism in
78 FTC-damaged concrete, especially under the unsaturated condition.

79 In the present paper a lattice network model in mesoscale is proposed which is able to simulate
80 the chloride transport process in unsaturated concrete and account for the damage induced by
81 freeze-thaw cycling. The formulation of the model and its implementation into a three-phase
82 composite structure of concrete is presented on the basis of reasonable quantification of transport
83 characteristics of water and chlorides into mortar, interfacial transition zone (ITZ) and cracks. The
84 application of the model is illustrated on a numerical example in which the concrete is subjected to
85 different FTCs in order to investigate the influence of damage or cracking on the chloride
86 penetration. The result of numerical analysis is compared with the previous test data published in
87 literature.

88 ***Principal Mechanisms for Chloride Ingress***

89 **Chloride binding capacity**

90 Under a natural and open condition, if the gravity or water pressure gradient is ignored, the
91 principal penetration processes for chlorides in concrete can be represented by diffusion (which is
92 caused by the concentration gradient of dissolved ions) and the convection as a result of bulk
93 moving water (which is induced by the capillary absorption). In addition, when chlorides penetrate
94 into concrete, it has been observed that some of the chlorides are chemically and physically bound
95 to the hydrated products of cement or the surfaces of some gel pores within concrete. This behavior
96 is called chloride binding capacity of concrete. Therefore, chloride in concrete is commonly
97 categorized as free and bound chloride. The total chloride concentration, C_t, can then be expressed
98 as

99 $$C_t = C_f + C_b \tag{1}$$

100 in which C_f is the free chloride concentration in kg/m^3 of the solution; C_b is the bound chloride
101 concentration. The chloride binding capacity is usually defined as the ratio of the change in the free
102 chloride concentration to the change in the total chloride concentration, which can be written as
103 follows:

104 $$\frac{\partial C_f}{\partial C_t} = \frac{1}{\frac{\partial C_t}{\partial C_f}} = \frac{1}{\frac{\partial (C_f + C_b)}{\partial C_f}} = \frac{1}{1 + \frac{\partial C_b}{\partial C_f}} \tag{2}$$

105 Here $\lambda = \frac{\partial C_b}{\partial C_f}$ is an experimentally obtained parameter. It is apparent that in concrete only the free
106 chloride is responsible for the steel corrosion because the bound chloride cannot migrate freely
107 through the concrete cover to reach the surface of embedded steel bars. Thereafter, in the current
108 study, the governing equation for chloride ingress, including diffusion and convection, is formulated
109 in terms of the free chloride concentration. Additionally, the chlorides brought by the concrete

mixtures are not considered here.

Water convection induced by capillary absorption

When a dried (or unsaturated) concrete is in contact with water, convection of bulk moving water induced by capillary absorption serves as the main carrier for chloride ingress. Generally, the water movement is not influenced by the existence of chloride ions. The flux of mass of chloride at any point in concrete, J_c, in kg/m^2.s, due to capillary absorption can be written as (Nagesh and Bhattacharjee 1998):

$$J_c = -C_f D_w(\theta)\frac{d\theta}{dx} \tag{3}$$

where $D_w(\theta)$ is the water or solution diffusivity in m^2/sec if the chloride ions are supposed to have the same transport speed with water; θ, here and elsewhere in the text, is the normalized water content, scaled to be zero and one for the initial (dried state) and saturated volumetric solution contents (i.e., volume of solution/bulk volume of concrete in m^3 of solution /m^3 of concrete), Θ_i and Θ_s, respectively; x is the space coordinate in concrete perpendicular to the exposed surface. Obviously, θ can be written as:

$$\theta = \frac{\Theta - \Theta_i}{\Theta_s - \Theta_i} \tag{4}$$

in which Θ is the volumetric solution content in m^3 of solution/m^3 of concrete. In experiments, the initial state Θ_i is specially reached by drying a specimen to constant weight at 105°C (in some experiments, lower than 105°C), so that, in this case Θ_i is close or equal to zero. The saturated state is reached by direct contact with an unlimited supply of water, which is approximately equal to the volume fraction porosity (Hall 1989). Apparently, the porosity of a material is an important parameter to influence the total water volume when exposed to the water source. Additionally, in the current study, the difference of diffusivity between salt solution and pure water is neglected

132 implying that $D_w(\theta)$ is independent of the solute concentration.

133 As has been pointed out, in absorption tests on capillary suction of NaCl solution, the speed of
134 the chloride ions ingress is lower than the speed of water due to the filter effect of the cement paste,
135 which is also called the retardation effect. This effect can be characterized by a retardation
136 coefficient R, defined as (Lunk 1998):

137 $$R = 1 - \frac{x_{\mathrm{cl}}}{x_w} \tag{5}$$

138 where x_{cl} is the mean chloride penetration depth and x_w is the mean water penetration depth.

139 In order to consider this effect, the flux of mass of chloride ions in Eq. (3) will be reduced by
140 multiplying the water diffusivity with the coefficient (1-R) (Roelfstra et al. 2004).

141 **Chloride diffusion under unsaturated state**

142 Because of the retardation effect of cement paste, the free chloride concentration is likely to vary
143 along the penetrating direction, even in the water-filled pores, so that a concentration gradient will
144 be generated. This concentration gradient, therefore, causes diffusion of chloride ions from higher
145 concentration to lower concentration. Usually the diffusion of chloride ions is formulated with
146 Fick's second law:

147 $$J_d = -D_{\mathrm{cl}}(\theta)\frac{dC_f}{dx} \tag{6}$$

148 where J_d is the flux of mass of chloride induced by the diffusion process; $D_{\mathrm{cl}}(\theta)$ is the chloride
149 diffusion coefficient in m^2/sec and is dependent on the water content.

150 The chloride diffusion in concrete is a humid process, which can occur only if water is present
151 in the pores of concrete (Saetta et al. 1993). Therefore, it has been stated that water content
152 (sometime referred as relative humidity) in concrete plays an important role in the chloride

diffusion process. Generally speaking, the diffusion coefficient of chloride decreases with the decrease of water content. Two different models to describe the interrelation between chloride diffusion coefficient and water content (or relatively humidity) are available currently.

The first model was developed by Saetta et al. (1993), using an *S*-shaped curve to account for the effect of relative humidity, RH, on the chloride diffusion coefficient, which can be expressed as:

$$\frac{D_{\mathrm{cl}}(\mathrm{RH})}{D_{\mathrm{cl1}}}=\left(1+\frac{(1-\mathrm{RH})^4}{(1-\mathrm{RH_c})^4}\right)^{-1} \tag{7}$$

where $D_{\mathrm{cl}}(\mathrm{RH})$, D_{cl1} are the chloride diffusion coefficient at any relative humidity and at the saturated state, respectively; $\mathrm{RH_c}$ is the critical relative humidity, at which $D_{\mathrm{cl}}(\mathrm{RH_c})=0.5D_{\mathrm{cl1}}$, and given as 75% by Saetta et al. (1993). When RH drops below $\mathrm{RH_c}$, the ion diffusivity shows a rough drop due to the loss of liquid connectivity inside the porous network. In terms of Eq. (7), Nielsen and Geiker (2003) experimentally determined $\mathrm{RH_c}$ to be 83% for a Portland cement mortar with *w*/*c*=0.5. De Vera et al. (2007) found that, for concrete with *w*/*c*=0.6, $\mathrm{RH_c}$ is fitted as 83.1%. In the current study, the curves of Eq. (7) with the previously proposed values of $\mathrm{RH_c}$ are presented in Fig. 2. To use Eq. (7), the relative humidity RH in Eq. (7) can be transferred into the normalized water content (θ) with the method proposed by Akita et al. (1994) as follows:

$$\theta = a_1 + a_2\mathrm{RH} + a_3\alpha + a_4\mathrm{RH}^2 + a_5\mathrm{RH}\alpha + a_6\alpha^2 + a_7\mathrm{RH}^3 + a_8\mathrm{RH}^2\alpha + a_9\mathrm{RH}\alpha^2 + a_{10}\alpha^3 \tag{8}$$

in which a_1~a_{10} are constants, and their values have been experimentally fitted as 33.4, 1.46, -0.287, -1.58×10^{-2}, -1.45×10^{-2}, 4.22×10^{-4}, 7.73×10^{-5}, 1.74×10^{-4}, -4.22×10^{-6} and 0, respectively; α is the water/cement ratio expressed in percentage (e.g. for *w*/*c*=0.5, the value of α is 50). The validity of Eq. (8) is illustrated in Fig. 1 by comparing the predicted results with available test data. It is evident that the method proposed by Akita et al. (1994) (Eq. (8)) is able to build an approximate relation between the RH and θ if ignoring the scatter of test results.

Saeki and Niki (1996) suggested another model with an empirical relationship to consider the

176 influence of water content on chloride diffusion coefficient:

177 $$\frac{D_{\mathrm{cl}}(\theta)}{D_{\mathrm{cl1}}} = 0.0032 \times 10^{0.025\theta} \tag{9}$$

178 $D_{\mathrm{cl}}(\theta)$ in Eq. (9) has the same definition as $D_{\mathrm{cl}}(\mathrm{RH})$ in Eq. (7) considering the relationship between
179 relative humidity RH and relative water content θ. The comparison of the above two models, as
180 well as compared with available test data, is depicted in Fig. 2. It can be seen that the curve
181 obtained from Eq. (7) with $\mathrm{RH_c}$=83% matches better with the experimental data than the curve from
182 Eq. (9). Thereafter, Eq. (7) with $\mathrm{RH_c}$=83% will be adopted in the subsequent analysis.

183 **Combined formulation of convection and diffusion**

184 Therefore, the total flux of chloride mass can be written as:

185 $$J = J_c + J_d = -\left[C_f D_w(\theta)(1-R)\frac{\partial \theta}{\partial x} + D_{\mathrm{cl}}(\theta)\frac{\partial C_f}{\partial x} \right] \tag{10}$$

186 Considering the mass balance of chloride ions in an infinitesimal volume of concrete, the following
187 equation can be obtained:

188 $$\frac{\partial C_t}{\partial t} = -\frac{\partial J}{\partial x} \tag{11}$$

189 By substituting Eq. (10) into Eq. (11) and applying Eq. (2), the governing equation for chloride
190 ingress in a 1-D case can thus be expressed as

191 $$\frac{\partial C_t}{\partial t} = \frac{\partial C_t}{\partial C_f}\frac{\partial C_f}{\partial t} = (1+\lambda)\frac{\partial C_f}{\partial t} = \frac{\partial}{\partial x}\left[C_f D_w(\theta)(1-R)\frac{\partial \theta}{\partial x} + D_{\mathrm{cl}}(\theta)\frac{\partial C_f}{\partial x} \right] \tag{12}$$

192 Rearranging Eq. (12), one can obtain

193 $$\frac{\partial C_f}{\partial t} = \frac{1-R}{1+\lambda} C_f \frac{\partial}{\partial x}\left[D_w(\theta)\frac{\partial \theta}{\partial x} \right] + \frac{1}{1+\lambda}\frac{\partial}{\partial x}\left(D_{\mathrm{cl}}(\theta)\frac{\partial C_f}{\partial x} \right) \tag{13}$$

194 The first term in the right-hand side of Eq. (13) represents the convection effect, i.e. chloride ingress
195 caused by water movement and the second term describes the diffusion process due to concentration
196 gradient. Water movement due to capillary absorption is usually described as follows:

$$\frac{\partial \theta}{\partial t} = \frac{\partial}{\partial x}\left[D_w(\theta) \frac{\partial \theta}{\partial x} \right] \tag{14}$$

Thus, Eq. (13) can be written as:

$$\frac{\partial C_f}{\partial t} = \frac{1-R}{1+\lambda} \frac{\partial \theta}{\partial t} C_f + \frac{1}{1+\lambda} \frac{\partial}{\partial x}\left(D_{\mathrm{cl}}(\theta) \frac{\partial C_f}{\partial x} \right) \tag{15}$$

To sum up, the penetration of chloride ions in an unsaturated concrete is governed by this coupled system of partial differential equation (PDEs), i.e. Eqs. (14) and (15). Moreover, one can clearly see that Eq. (14) and the second term of Eq. (15), representing the two mechanisms of convection and diffusion respectively, have the similar form. Therefore, when the coupled PDEs are applied numerically, two consecutive steps are usually adopted with in a time interval (time step) to solve this problem: the first step is to solve Eq. (14) for water movement; the second step is to solve Eq. (15) following the results of water absorption in the first step to obtain the chloride concentration (Ababneh et al. 2003). It should be pointed out that an iteration process should be used to solve Eq. (14) (the first step) because $D_w(\theta)$ is strongly dependent on the relative water content, which will be argued in the following section.

Transport of capillary water

When concrete is assumed to be fully hydrated, implying no further water consumed during the ingress process, transport of capillary water can be described in terms of volume fraction of pore water by Richards' equation (Ozbolt et al. 2010). The equation for unsaturated flow through porous media is expressed as:

$$\frac{\partial \theta}{\partial t} = \nabla \cdot \left(D_w(\theta) \nabla \theta \right) \tag{16}$$

For a 1-D semi-infinite system subject to a boundary condition θ=1 at x=0 and an initial condition θ=0, x>0, t=0 (uniform initial water content within the sample of material), Eq. (16) turns into Eq. (14). By applying the Boltzmann's transformation, i.e., introducing the Boltzmann variable,

$\phi = x.t^{-1/2}$, the partial differential Eq. (14) can be reduced to an ordinary boundary-value problem (Lockington, et al. 1999):

$$-\frac{1}{2}\phi\frac{d\theta}{d\phi} = \frac{d}{d\phi}\left(D_w(\theta)\frac{d\theta}{d\phi}\right) \tag{17}$$

with $\theta=1$ for $\phi=0$, and $\theta=0$ as $\phi\to\infty$.

The functional relationship between D_w and θ is strongly non-linear, which is commonly approximated by the exponential-law (Hall 1989; Hall 1994; Lockington et al. 1999):

$$D(\theta) = D_0 e^{n\theta} \tag{18}$$

in which D_0 and n are empirically-fitted constants. Eq. (18) is widely utilized because of its relatively simple expression and rather narrow range of parameter n (6 to 8 by Hall (1989)). The cumulative water absorption of a sample, i, increases as the square root of the elapsed time t:

$$i = St^{1/2} \tag{19}$$

in which S is defined as the sorptivity of a porous materials, and regarded as the rate of water uptake by the material when exposed to a water resource. In some literatures, it is also named as the coefficient of capillary suction (Wittmann et al. 2006). Obviously from Eq. (19), S can be easily determined from the slope of the i versus $t^{1/2}$ curve, where i is measured in experiment as $i=\Delta w/A\rho_w$ (in which Δw is the increase in weight, A the cross-sectional area and ρ_w the density of water).

An approach was proposed to determine the constants n and D_0 with the experimentally regressed value of S (Lockington et al. 1999). In their method, the constant n is taken a universal value as 6.0, and then D_0 can be approximately estimated by:

$$D_0 = s^2/123.131 \tag{20}$$

where $s=S/(\Theta_s-\Theta_i)$, is the normalized sorptivity. The rationality of Lockington (1999)'s method has been illustrated in a previous work (Wang and Ueda 2011).

Lattice network model on mesoscale

One of the advantages of mesoscale modeling of strongly heterogeneous materials such as concrete is that it can particularly represent the characteristics of interface between different materials. For example, recent studies have began to treat concrete as a three-phase composite material, consisting of coarse aggregates, mortar matrix and the interfacial transition zones (ITZs) between the aggregate particles and the surrounding mortar. Compared with the bulk cement paste, the ITZ has higher w/c and porosity. Except the HPC (High Performance Concrete), the ITZ is likely to be cracking when subjected to load or environmental attack. From this point of view, the ITZ is often regarded as a zone of weakness in both the mechanical and transport properties. To precisely predict the transport properties of concrete, especially to account for the influence of damage or cracking, the ITZ should be separately taken into account and treated as the critical phase of concrete.

Mesoscale structure of concrete

The size distribution of coarse aggregates in a geometrical domain is generated in terms of the Fuller's curve for aggregate gradation. The Fuller's curve is usually given by the following formula:

$$P_i = \left(\frac{d_i}{D_{\max}} \right)^n \times 100\% \tag{21}$$

where $D_{\max}$ represents the maximum aggregate grain size; d_i represents a given particle size, and P_i denotes the percent of the aggregate that is finer than d_i. A typical value for the exponent n is 0.45 or 0.50. On the basis of Fuller's curve, Walraven et al. (1981) transferred this 3-D gradation curve into a 2-D aggregate distribution model for the cross section of a concrete sample, i.e. the area percentage of the aggregates with diameter less than D_0 can be written as:

$$P_c(D < D_0) = P_k(1.065 D_0^{0.5} D_{\max}^{-0.5} - 0.053 D_0^4 D_{\max}^{-4} - 0.012 D_0^6 D_{\max}^{-6} - 0.0045 D_0^8 D_{\max}^{-8} + 0.0025 D_0^{10} D_{\max}^{-10}) \tag{22}$$

in which D_0 is one of the aggregate diameter in the gradation series; P_k is the volume fraction of coarse aggregate.

264 In this study, a standard pseudo-random number generator is used to produce probabilities from
265 which the diameter of the aggregate is determined. This procedure is repeated until the calculated
266 volume fraction of aggregates by Eq. (22) is obtained. After accomplishing the database of
267 aggregate particles, the particles are randomly placed one by one into the domain of the concrete
268 sample in such a way that there is no overlapping with particles already placed (Grassl and Pearce
269 2010; Wang et al. 1999). An example of the generated concrete sample by the above procedure is
270 shown in Fig. 3 with coarse aggregate volume fraction of 39.5% and maximum and minimum
271 diameters of 20 mm and 4 mm respectively.

272 **Lattice network model**

273 In the past few years, it has been proposed that on the mesoscale level, mass transport in concrete
274 can be described by means of lattice-type model. This type of model is categorized as a discrete
275 numerical method and has the advantage of mesh-independence and accurate descriptions of basic
276 properties of the continuum response (Sadouki and Van Mier 1997; Grassl 2009). In our previously
277 published paper (Wang and Ueda 2011), the lattice network model was established to simulate
278 capillary water transport process by concrete on the basis of Voronoi tessellation. Fig. 4 illustrates
279 the composition of lattice network of a concrete specimen on mesoscale. In Fig. 4, polygons with
280 dotted sides are the Voronoi elements after meshing the specimen. By connecting the nodes in
281 Voronoi diagram (nuclei of Voronoi polygons and the intermediate points on edges of the Voronoi
282 polygons), a network with five types of lattice elements is established with respect to their position
283 falling in the mesostructure of concrete (see Fig. 4a). Each type of lattice element has their unique
284 transport property. When concrete is damaged due to mechanical loading or environmental action
285 (e.g., freeze and thaw cycling), cracks are always supposed to generate and propagate along the
286 joint edge of two neighbouring Voronoi elements (see Fig. 4b). In other words, the cracks are only

allowed to present on the dotted lines. It should be pointed out that the 3-D configuration of cracks is not considered due to the 2-D analysis nature. Therefore, in the present approach, the crack depth perpendicular to mass moving direction is assumed to be same with thickness of the specimen, which was usually set as unit thickness. As a result, the lattice elements along cracks will be given their cross-sectional area and diffusivity in terms of the crack openings. Only an overview of this approach is briefly given here. Additional details, such as those related to Voronoi element construction, lattice element meshing method and the discrete form of governing equation have been reported by Wang et al. (2008) and Wang and Ueda (2011).

The use of an irregular lattice network for the description of water movement in uncracked concrete has been successfully implemented (Wang and Ueda, 2011). In the current work, the effect of cracks caused by FTCs attack is under the consideration.

Chloride penetration of undamaged concrete

Chloride diffusion coefficient of the ITZ

As already mentioned, chloride ions penetrate faster in the ITZ than in the bulk cement paste. Numerous studies have been carried out to investigate and quantify the effect of ITZs on the transport properties of mortar and concrete. The diffusion coefficients of the ITZ, as well as its thickness obtained from the literatures are listed in Table 1. Although their conclusions are not in full agreement with each other, it can be generally summarized that D_{ITZ} is usually less than 16 times of that of cement paste, especially in most cases no more than 10 times. Moreover, because the diffusion coefficient of mortar has the same magnitude of order as that of cement paste (Caré 2003; Caré and Hervé 2004), the D_{ITZ}, in the calculation process of this paper, is roughly assumed as 10 times of that corresponding to mortar. It means that the diffusion coefficient for lattice

elements on the aggregate-mortar boundary is taken as 10 times higher than that for the lattice elements within mortar.

Numerical example- initial and boundary conditions

The modeling approach described above, which was implemented by C++ language and performed on a personal computer on Windows, is applied to a NaCl solute absorption problem. The experimental study on this numerical example has been performed by Wittmann et al. (2006) to investigate the freezing-thawing damage on water and chloride transport properties of concrete. In the current analysis, the water-to-cement ratio is assumed to be 0.6 in order to coincide with that used in test. In the domain of the specimen, the volume fraction of coarse aggregate is 49%, which is very close to that used in the experiment. The Voronoi meshing diagram of the sample, as well as the illustration of boundary condition, is shown in Fig. 5, which is modeled with 844 Voronoi elements and 8961 lattice elements (but for sake of clearness, the lattice elements are not depicted). In the experimental program, concrete cubic specimens with an edge length of 100 mm were cut into two halves (i.e. the thickness of each slice is 50 mm). After adequately cured in the humid curing room, the samples were further stored under laboratory conditions at 20 ± 3 °C and 50 % RH for another 21 days. And then, they were dried in an aerated oven at a temperature of 50°C for 24 hrs before put in contact with NaCl solution with a concentration of 3%. It was found that there was no further apparent weight loss for the samples undergone the above drying operation. During the penetration test, the four lateral sides of the slice were sealed with wax in order to have one directional flow from the bottom surface through the specimen. The schematic representation of the experimental set-up can be referred to Wittmann et al. (2006). To fit the test conditions, the bottom and top surfaces of the specimen are treated to be exposed to chloride solution and to fully dried atmosphere respectively, whereas the two side surfaces are completely sealed. In terms of the above

drying procedure and thin thickness of the slice, the sample can be assumed to fully dried before contacting to water solution. As a result, the initial and boundary condition for transport of capillary water are taken as follows: $\theta(x)$=0.0, for t=0; $\theta(x_b)$=1.0, for t>0; x_b is the coordinate of the nodes of lattice elements that are exposed to the solution. It implies that on the exposed surface, concrete is assumed to be fully saturated. Therefore, the chloride concentration on the exposed surface was determined as 4.86×10^{-3} g/cm^3 for undamaged concrete in terms of the concrete porosity, which was estimated as 26.7% with w/c=0.6 by means of the Powers' model (Hansen 1986). It was kept constant in the 24 hours' analysis by assuming that the 3% NaCl solution (with chloride concentration in the solution of 1.82×10^{-2} g/cm^3) completely fill in the pores at the very thin surface layer of concrete. It should be noted that the chloride concentration on the exposed surface, is varied with the damage degree of concrete because the damage can result in a porosity increase. In addition, from the test data of all samples, constant chloride content (0.07% by weight of concrete) was observed in deep position along penetration direction, at which the chlorides were unreachable in 24 hours. This implies that initial chloride content was present in the concrete mixture, which was estimated to be 1.68×10^{-3} g/cm^3 if the concrete density is taken 2.4 g/cm^3. To summarize, for chloride transport, the initial and boundary conditions are: $C_f(x)=1.68\times10^{-3}$ g/cm^3 for t=0, which was observed from the experimental results; $C_f(x_b)=4.86\times10^{-3}$ g/cm^3 of concrete, for t>0. The filter effect, making the chloride front slower than water penetration, is also taken into account with the coefficient of R=0.7.

Predicted result of the chloride profile

As the water absorption have been analyzed in a previous paper (Wang and Ueda, 2011), only the distribution of chloride will be argued here, and shown in Fig. 6. The effect of coarse aggregates on the chloride penetration front can be clearly observed in the penetration area: on one hand, the

355 coarse aggregates, especially those with relatively larger size can “block” the moving chlorides due
356 to their lower permeability; on the other hand, the presence of ITZs, which have higher porosity,
357 will contribute to facilitating the penetration of chlorides. Therefore, from Fig. 6, one can see that
358 the chloride concentration in the area behind coarse aggregates is much lower than that in the area
359 of surrounding mortar matrix. This phenomenon has been experimentally observed and considered
360 to cause the scatter in the depths of chloride penetration even within the same sample (Rodriguez
361 and Hooton 2003)

362 Fig. 7 provides the comparison of chloride profiles in concrete between the predicted results by
363 the lattice network model and the experimental data obtained by Wittmann et al. (2006). It can be
364 seen that in this example, after 24 hrs exposure to NaCl solution, the predicted chloride profile is in
365 good agreement with the experimental measurement.

366 ***Chloride Penetration of Freeze-thaw damaged concrete***

367 **Cracks induced by freeze-thaw cycling**

368 Recent studies have shown that subjecting to freeze-thaw damage can result in the increase of
369 permeability of concrete due to the occurrence of new cracks and connectivity of originally existing
370 microcracks (Jacobsen et al. 1996; Yang et al. 2006). For example, Jacobsen et al. (1996) observed
371 that the freeze-thaw cycling can increase the chloride penetration rate up to about 2.5 to 8 times
372 after 31 to 95 FTCs when compared with the undamaged concrete. It also indicates that the internal
373 cracking of concrete induced by freeze-thaw cycling is significantly dependent on the number of
374 cycles. Therefore, after different FTCs, the knowledge on internal cracks, e.g., the crack distribution
375 (numbers and location) and crack width should be investigated and made clear so as to estimate
376 their effects on chloride transport.

377 Contrary to the research effort on freeze-thaw mechanism, it seems that in the past, studies on

the characteristics of FTC-induced cracks were mostly focused on the qualitative interpretation, but few could give a precise and quantitative description of the cracks. For instance, Jacobsen et al. (1996) performed the rapid freeze-thaw experiment on a non-air entrained concrete with w/c of 0.4 and measured an ultimate volume increase as 2.9% after 95 FTCs by weighing the frosted specimen in air and water respectively. Hasan et al. (2004) conducted a freezing-thawing test on the non-air entrained concrete (w/c=0.5) in a climate chamber. In this experiment, the strain variation, defined as the plastic tensile strain, was measured during the freezing-thawing process and regarded as the evaluation of damage degree. Therefore, for the purpose of application of numerical models, it is necessary to convert the above test measurements into the cracking information.

For a prismatic specimen with the initial size of $V_0=L_1\times L_2\times L_3$, the increase length of each side due to freeze-thaw cycling is set as ΔL_1, ΔL_2 and ΔL_3, then the increased volume ΔV may be calculated as:

$$\Delta V=(L_1+\Delta L_1)\,(L_2+\Delta L_2)\,(L_3+\Delta L_3)-V_0 \tag{23}$$

Then the ratio of volume increase is written as:

$$\frac{\Delta V}{V_0}=\frac{(L_1+\Delta L_1)(L_2+\Delta L_2)(L_3+\Delta L_3)}{L_1L_2L_3}-1=\left(1+\frac{\Delta L_1}{L_1}\right)\left(1+\frac{\Delta L_2}{L_2}\right)\left(1+\frac{\Delta L_3}{L_3}\right)-1 \tag{24}$$

Here, a uniform assumption is typically given that freeze-thaw cycling may cause the same expansion along each direction. Thus the above equation can be written as:

$$\frac{\Delta V}{V_0}=(1+\varepsilon)(1+\varepsilon)(1+\varepsilon)-1=(1+\varepsilon)^3-1 \tag{25}$$

in which ε is the plastic strain induced by freeze-thaw cycling in any direction. Reversely, according to Eq. (25), when the volume increase is measured, the plastic strain of a specimen can be estimated as:

$$\varepsilon=\sqrt[3]{1+\frac{\Delta V}{V_0}}-1 \tag{26}$$

400 The volume increase and plastic strain derived from experimental data (Hasan et al. 2004;
401 Jacobsen et al. 1996) based on Eq. (26) are given in Table 2, together with their originally measured
402 results.

403 From Table 2 it can be observed that results from the two tests differ too much up to an
404 order-of-magnitude variation. The most significant reason seems to be attributed to the different
405 freezing-thawing process and deformation measuring method as explained above. However, it
406 should be noted that in Jacobsen et al.'s experiment, not only the volume increase was measured but
407 also the crack density and crack width were also evaluated with the scanning electron microscope
408 (SEM). Further more, the calculated crack width using the measured volume increase, as shown in
409 Table 2, was proved to be in good accordance with the SEM observation (Jacobsen et al. 1995). And
410 recently, a similar crack width magnitude order was also observed by using the SEM technology
411 (Yang et al. 2006). Therefore, in this study, the width of FTC-induced cracks will be determined
412 based on experimental data obtained by Jacobsen et al. (1996).

413 In addition to the crack width, observation with SEM reveals that after freeze-thaw exposure,
414 cracks mostly occur in the interface between cement paste and aggregate (Jacobsen et al. 1995;
415 1996; Yang et al. 2006). Based on this fact, in the lattice network model, all the cracks are assumed
416 to be present around the coarse aggregates and the cross-sectional area of lattice elements on the
417 ITZs (see Fig. 4) will be adjusted according to the crack width. And then the corresponding
418 diffusivity of water and chloride through these elements will be determined using the approach in
419 the following sections. The influence of FTC-induced cracking and the above modeling method
420 have been demonstrated in a previous paper in terms of a pure diffusion process of chloride under
421 saturated condition (Wang and Ueda 2009). It was found that the diffusion coefficient of concrete
422 after frost attack is increased with the increase of freezing-thawing cycles.

Diffusivity of water and chlorides through cracks

Because few attempts have been done to quantify the process for water transport through a single crack, Nakamura et al. (2006) suggested that, under the saturated condition, the water transport coefficient through a single crack could be empirically set as 1.0×10^5 mm^2/day (i.e., 4200 mm^2/hr).

Presently, there are a number of experimental investigations available for assessing the penetration rate of chlorides through a single crack. This is well documented in the literatures (Djerbi et al. 2008; Kato et al. 2005; Takewaka et al. 2003; Ismail et al. 2008; Rodriguez and Hooton 2003). Sahmaran (2007) found that that for crack width less than 135 μm, the effect of crack width on the diffusion coefficient of mortar was marginal, whereas for crack width higher than 135 μm the diffusion coefficient increased rapidly. This threshold value was found to be 75 μm by Kato et al. (2005). Because the width of a crack induced by freeze-thaw is usually very small (e.g., the order of magnitude was measured as about 10 μm, see Table 2), the diffusion coefficient of chloride transport through a crack is assumed to be independent to the crack width and set as 3000 mm^2/hr based on the previous findings (Wang and Ueda 2011). Moreover, for one crack lattice element, the smooth surface is assumed since it has been experimentally observed that the chloride diffusion in cracked concrete is independent of the crack surface roughness (Rodriguez and Hooton 2003).

Water and chloride distribution in damaged concrete

The parameters used for numerical simulation of water and chloride transport through freezing-thawing damaged concrete are summarized in Table 3. The contacting time of sample to water is assumed as 24 hrs long. Wittmann et al. (2006) conducted the research on water and chloride penetration in concrete after 50 and 150 FTCs, so that their experimental data will be used

445 to verify the numerical result. After subjected to 50 and 150 FTCs, the width of microcracks within
446 concrete is taken as 8 μm and 15 μm respectively, which are deduced from the observation of
447 Jacobsen et al (1996). The distribution of water content over the depth of the specimen after 8 and
448 24 hrs' exposure is shown in Fig. 8. Moreover, the numerical results of cumulative absorbed water
449 for concrete samples after different FTCs are compared with the experiment data and depicted in
450 Fig. 9. It can be seen that the penetration of water is much faster and deeper in cracked than in
451 un-cracked concrete. The amount of up-taken water by the sample is found to increase with the
452 increase of FTCs, which is in good agreement with experimental observation. This result can be
453 attributed to the formation of more penetration paths and connectivity of the initial microcracks
454 when subjected to the action of freezing-thawing. To further illustrate this phenomenon, the
455 relationship between water content θ and Boltzmann variable ϕ of concrete subjected 50 and 150
456 FTCs, as well as that without damage, is shown in Fig. 10. It is noted that at the same value of
457 Boltzmann variable, the water content has a notable increase after subjected to freeze-thaw cycling.
458 Similarly, Fig. 11 shows the comparison of the model predictions and experimental results for
459 the chloride profiles after 50 and 150 FTCs. Comparing the distribution of chlorides after subjecting
460 to different FTCs (see Figs. 7 and 11), it can be seen that the chlorides penetrate deeper with
461 increase of FTCs. A similar conclusion was drawn in experiments (Wittmann et al. 2006). The
462 agreement between the prediction of numerical model and test data illustrates that the lattice
463 network model, combined with the foregoing formulation in this paper, can successfully simulate
464 the chloride penetration in unsaturated, FTC-damaged concrete.

465 ***Summary and Conclusions***

466 In the present paper, a numerical simulation approach in mesoscale with the lattice network model
467 is reported to evaluate the chloride ions penetration process within unsaturated concretes before and

after subjected to the freezing-thawing cycles (FTCs). The following conclusions can be drawn:

1) In the mesoscale, concrete is represented as a three-phase composite, i.e., the mortar matrix, aggregate particles and interfacial transition zones (ITZs), so that it is possible to involve separate material models (e.g., transport model) for each phase. The strategy of Voronoi diagram is adopted that is able to account for the damage or cracking with the concept of discrete cracks. On the basis of Voronoi tessellation of a concrete domain (uncracked or cracked), an irregular network composing of various types of lattices is built up to describe the water and chlorides transport.

2) Under unsaturated state, chloride penetration in concrete is attributed to two mechanisms, i.e. convection (water absorption) and diffusion. The mathematical formulation of this combined process is proposed and implemented into the lattice network, and then solved by two consecutive steps separately.

3) FTC-induced damage can be represented by a uniformly distributed and connected crack network throughout the concrete. As a result, both the water absorption and chloride penetration will be accelerated after subjected to FTCs. In this study, the features of microcracks, including crack distribution and widths, are clarified by investigating and analyzing the available experimental observations. After applying the lattice network model to the FTC-damaged concrete, the distribution of water and chloride over the depth of the specimen are quantitatively obtained. It is observed that the penetration of water and chloride is faster and deeper in damaged than in undamaged concrete. The damage of concrete also significantly increases the amount of up-taken water.

4) The lattice network model, coupled with the mesoscale structure of concrete, seems to provide a realistic tool for simulating the chloride penetration process in intact or damaged concrete

material since the predicted chloride profiles agree well with experimental data. Therefore, it may be hoped that the attempt in this paper could be helpful to reduce the experimental time and errors, and further be used to facilitate the service life prediction of concrete structures subjected to the combination action of freeze-thaw cycling and salt attack. It should also be pointed out that further work, especially the quantification of FTC-induced damage and media transport property through crack, is needed in order to increase the precision of simulation.

Acknowledgements

This study was supported by the National Natural Science Foundation of China (Grant No. 51378090), the Open Research Fund Program of State Key Laboratory of Hydroscience and Engineering (sklhse-2011-C-03) and the Asia-Africa Science and Technology Strategic Cooperation Promotion Program by the Special Coordination Funds for Promoting Science and Technology of Japan.

References

Ababneh, A., Benboudjema, F. and Xi, Y. (2003). "Chloride penetration in nonsaturated concrete." *J. Mater. Civil Eng.*, 15(2), 183-191.

Akita, H., Fujiwara, T. and Osaka, Y. (1994). "An analytical method of moisture transfer within concrete due to drying." *J. Mater. Concr. Struct. Pav.*, 23(490), 101-110. (in Japanese)

Aldea, C-M., Shah, S. P. and Karr, A. (1999). "Effect of cracking on water and chloride permeability of concrete." *J. Mater. Civil Eng.*, 11(3), 181-187.

Bentz, D. P., Detwiler, R. J., Garboczi, E. J., Halamickova, P. and Schwartz, L. M. (1997). "Muti-scale modeling of the diffusivity of mortar and concrete." In: L.O. Nilsson and J. P. Ollivier, Eds., *Proc. of Chloride Penetration into Concrete*, Saint-Rémy-lès-Chevreuse, France, RILEM

publications, 85-94.

Boddy, A., Bentz, E., Thomas, M. D. A. and Hooton, R. D. (1999). "An overview and sensitivity study of a multimechanistic chloride transport model." *Cem. Concr. Res.*, 29(6), 827-837.

Breton, D., Ollivier, J. P. and Ballivy, G. (1992). "Diffusivity of chloride ions in the transition zone between cement paste and granite." In: J. C. Maso, Ed., *Interfaces between Cementitious Composites*, E & F. N. Spon, London, 279-288.

Caré, S. (2003). "Influence of aggregates on chloride diffusion coefficient into mortar." *Cem. Concr. Res.*, 33(7), 1021-1028.

Caré, S. and Hervé, E. (2004). "Application of an n-phase model of the diffusion coefficient of chloride in mortar." *Transport Porous Med.,* 56(2), 119-135.

Delagrave, A., Marchand, J. and Samson, E. (1996). "Prediction of diffusion coefficients in cement-based materials on the basis of migration experiments." *Cem. Concr. Res.*, 26(12), 1831-1842.

Climent, M. A., de Vera, G., Lopez, J. F., Viqueira, E., and Andrade, C. (2002). "A test method for measuring chloride diffusion coefficients through nonsaturated concrete. Part I: The instantaneous plane source diffusion case." *Cem. Concr. Res.*, 32(7), 1113-1123.

de Vera, G., Climent, M. A., Viqueira, E., Anton, C. and Andrade, C. (2007). "A test method for measuring chloride diffusion coefficients through partially saturated concrete. Part II: The instantaneous plane source diffusion case with chloride binding consideration." *Cem. Concr. Res.*, 37(5), 714-724.

Djerbi, A., Bonnet, S., Khelidj, A. and Baroghel-bouny, V. (2008). "Influence of traversing crack on chloride diffusion into concrete." *Cem. Concr. Res.*, 38(6), 877-883.

Gérard, B., Breysse, D., Ammouche, A., Houdusse, O. and Didry, O. (1996). "Cracking and

536 permeability of concrete under tension." *Mater. Struct.*, 29(3), 141-151.

537 Grassl, P. (2009). "A lattice approach to model flow in cracked concrete." *Cem. Concr. Compos.*,

538 31(7), 454-460.

539 Grassl, P. and Pearce, C. (2010). "Mesoscale approach to modeling concrete subjected to

540 thermomechanical loading." *J. Eng. Mech.*, 136(3), 322-328.

541 Hall, C. (1989). "Water sorptivity of mortar and concretes: a review." *Mag. Concr. Res.*, 41(147),

542 51-61.

543 Hall, C. (1994). "Barrier performance of concrete: A review of fluid transport theory." *Mater. Struct.*,

544 27(2), 291-306.

545 Hansen, T. C. (1986). "Physical structure of hardened cement paste: a classical approach". *Mater.*

546 *Struct*., 19(114), 423-436.

547 Hasan, M., Okuyama, H., Sato, Y. and Ueda, T. (2004). "Stress-strain model of concrete damaged

548 by freezing and thawing cycles." *J. Adv. Concr. Tech.*, 2(1), 89-99.

549 Ishida, T., Iqbal, P. O. N. and Anh, H. T. L. (2009). "Modeling of chloride diffusivity coupled with

550 non-linear binding capacity in sound and cracked concrete." *Cem. Concr. Res.*, 39(10), 913-923.

551 Ismail, M., Toumi, A., Francois, R. and Gagne, R. (2008). "Effect of crack opening on the local

552 diffusion of chloride in cracked mortar samples." *Cem. Concr. Res.*, 38(8-9), 1106-1111.

553 Jacobsen, S., Gran, H. C., Sellevold, E. J. and Bakke, J. A. (1995). "High strength

554 concrete-freeze/thaw testing and cracking." *Cem. Concr. Res.*, 25(8), 1775-1780.

555 Jacobsen, S., Marchand, J. and Boisvert, L. (1996). "Effect of cracking and healing on chloride

556 transport in OPC concrete." *Cem. Concr. Res.*, 26(6), 869-881.

557 Jaffer, S. J. and Hansson, C. M. (2008). "The influence of cracks on chloride-induced corrosion of

558 steel in ordinary Portland cement and high performance concretes subjected to different loading

559 conditions." *Corr. Sci.*, 50 (12), 3343-3355.

560 Kato, Y. and Uomoto, T. (2005). "Modeling of effective diffusion coefficient of substances in
561 concrete considering spatial properties of composite materials." *J. Adv. Concr. Tech.*, 3(2), 241-251.

562 Kelham, S. (1988). "A water absorption test for concrete." *Mag. Concr. Res*., 40(143), 106-110.

563 Lockington, D., Parlange, J. -Y. and Dux, P. (1999). "Sorptivity and the estimation of water
564 penetration into unsaturated concrete." *Mater. Struct*., 32(5), 342-347.

565 Lunk, P. (1998). "Penetration of water and salt solutions into concrete by capillary suction." *J. of*
566 *Restor. Build. Monu.*, (4), 399-422.

567 McCarter, W. J., Ezirim, H. and Emerson, M. (1992). "Absorption of water and chloride into
568 concrete." *Mag. Concr. Res.*, 44(158), 31-37.

569 Nagesh, M. and Bhattacharjee, B. (1998). "Modelling of chloride diffusion in concrete and
570 determination of diffusion coefficients." *ACI Mate. J*., 95(2), 113-120.

571 Nakamura, H., Srisoros, W., Yashiro, R. and Kunieda, M. (2006). "Time-dependent structural
572 analysis considering mass transfer to evaluate deterioration process of RC structures." *J. Adv. Concr.*
573 *Tech.*, 4(1), 147-158.

574 Neithalath, N. (2006). "Analysis of moisture transport in mortars and concrete using
575 sorption-diffusion approach." *ACI Mate. J.*, 103(3), 209-217.

576 Nielsen, E. and Geiker, M. R. (2003). "Chloride diffusion in partially saturated cementitious
577 material." *Cem. Concr. Res.*, 33(1), 133-138.

578 Oh, B. H. and Jang, S. Y. (2004). "Prediction of diffusivity of concrete based on simple analytic
579 equations." *Cem. Concr. Res.*, 34(3), 463-480.

580 Ozbolt, J., Balabanic, G., Periskic, G. and Kuster, M. (2010). "Modelling the effect of damage on
581 transport processes in concrete." *Constr. Build. Mater.*, 24(9), 1638-1648.

582 Qi, C. (2003). “Quantitative assessment of plastic shrinkage cracking and its impact on the
583 corrosion of steel reinforcement.” Ph.D thesis, Purtue Univ., West Lafayette, Ind.
584 Rodriguez, O. G. and Hooton, R. D. (2003). “Influence of cracks on chloride ingress into concrete.”
585 *ACI Mater. J.*, 100(2), 120-126.
586 Roelfstra, G., Hajdin, R., Adey, B. and Bruhwiler, E. (2004). “Condition evolution in bridge
587 management systems and corrosion-induced deterioration.” *J. Brid. Eng.*, 9(3), 268-277.
588 Sadouki, H. and Van Mier, J.G. M. (1997). “Meso-level analysis of moisture flow in cement
589 composites using a lattice-type approach.” *Mater. Struct.*, 30(10), 579-587.
590 Saeki, T. and Niki, H. (1996). “Migration of chloride ions in non-saturated mortar.” *Proc. Japan*
591 *Concr. Ins*., 18(1), 963-968. (in Japanese)
592 Saetta, A. V., Scotta, R. V. and Vitaliani, R. V. (1993). “Analysis of chloride diffusion into partially
593 saturated concrete.” *ACI Mater. J*., 90(5), 441-451.
594 Sahmaran, M. (2007). “Effect of flexure induced transverse crack and self-healing on chloride
595 diffusivity of reinforced mortar.” *J. Mater. Sci.*, 42 (22), 9131-9136.
596 Sahmaran, M., Li, M. and Li V. C. (2007). “Transport properties of engineered cementitious
597 composites under chloride exposure.” *ACI Mater. J.*, 104(6), 604-611.
598 Schiessl, P. and Raupach, M. (1997). “Laboratory studies and calculations on the influence of crack
599 width on chloride-induced corrosion of steel in concrete.” *ACI Mater. J.*, 94 (1), 56-62.
600 Shane, J. D., Mason, T. O., Jennings, H. M., Garboczi, E. J. and Bentz, D. P. (2000). “Effect of the
601 interfacial transition zone on the conductivity of Portland cement mortar.” *J. Amer. Ceram. Soc.*,
602 83(5), 1137-1144.
603 Takewaka, K., Yamaguchi, T. and Maeda, S. (2003). “Simulation model for deterioration of
604 concrete structures due to chloride attack.” *J. Adv. Concr. Tech.*, 1(2), 139-146.

605 Ueda, T., Hasan, M, Nagai, K., Sato, Y. and Wang, L. (2009). “Mesoscale simulation of influence
606 of frost damage on mechanical properties of concrete.” *J. Mater. Civil Eng.*, 21(6), 244-252.
607 Walravent, J. C. and Reinhard, H. W. (1981). “Theory and experiments on the mechanical behavior
608 of cracks in plain and reinforced concrete subject to shear loading.” *HERON*, 26(1), 1-68.
609 Wang, K., Jansen, D. C. and Shah, S. P. (1997). “Permeability study of cracked concrete.” *Cem.*
610 *Concr. Res.*, 27(3): 381-393.
611 Wang, L. C., Soda, M. and Ueda, T. (2008). “Simulation of chloride diffusivity for cracked concrete
612 based on RBSM and truss network model.” *J. Adv. Concr. Tech.*, 6(1), 143-155.
613 Wang, L. C. and Ueda, T. (2009). “Mesoscopic simulation of chloride ions diffusion in
614 frost-damaged concrete.” *Int. J. Model., Ident. Control.*, 7(2), 148-154.
615 Wang, L. C. and Ueda, T. (2011). “Mesoscale modeling of water penetration into concrete by
616 capillary absorption.” *Ocean Eng.*, 38(4), 519-528.
617 Wang, Z. M., Kwan, A. K. H. and Chan, H. C. (1999). “Mseoscopic of study of concrete I:
618 Generation of random aggregate structure and finite element mesh.” *Comp. struct*., 70(5), 533-544.
619 Wittmann, F. H., Zhang, P. and Zhao, T. (2006). “Influence of combined environmental loads on
620 durability of reinforced concrete structures.” *Restor. Build. Monu.*, 12(4), 349-362.
621 Yang, C. C. (2003). “Effect of the interfacial transition zone on the transport and the elastic
622 properties of mortar.” *Mag. Concr. Res.*, 55(4), 305-312.
623 Yang, Z., Weiss, W. J. and Olek, J. (2006). “Water transport in concrete damaged by tensile loading
624 and freeze-thaw cycling.” *J. Mater. Civil Eng.*, 18(3), 424-434.

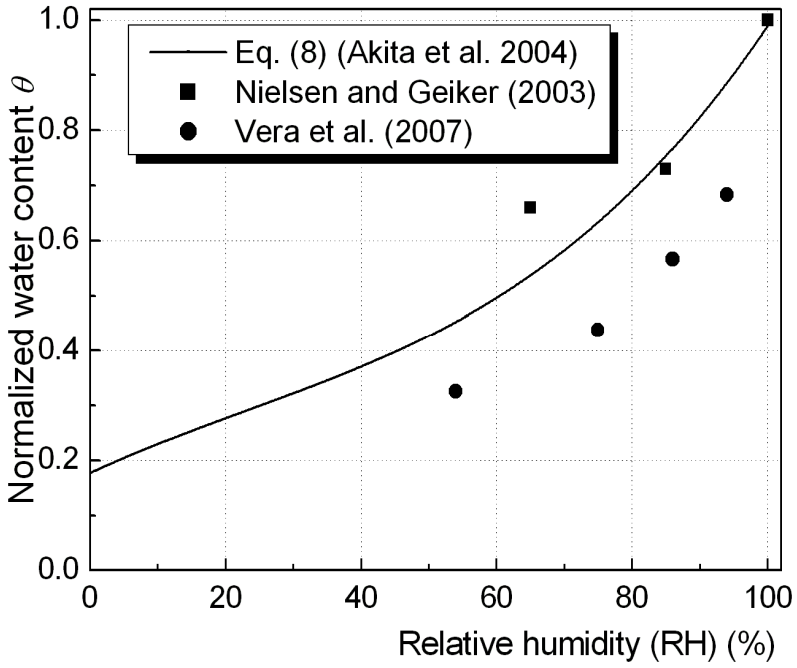

Fig. 1. Relationship between relative humidity (RH) and normalized water content θ

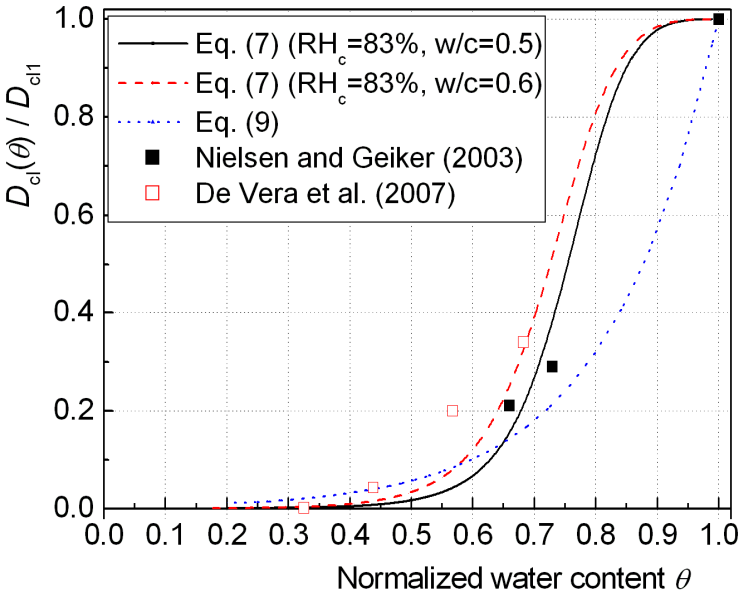

Fig.2. Comparison of models on chloride diffusion coefficient versus water content

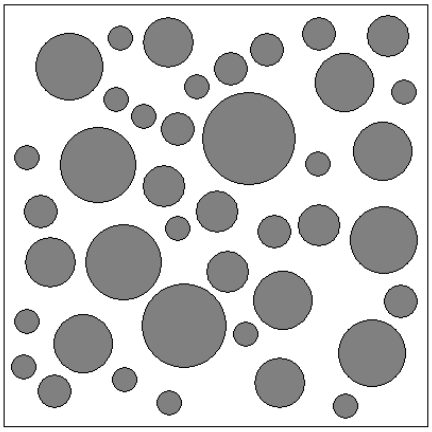

Fig. 3. The 2-D mesoscale model of a concrete cube

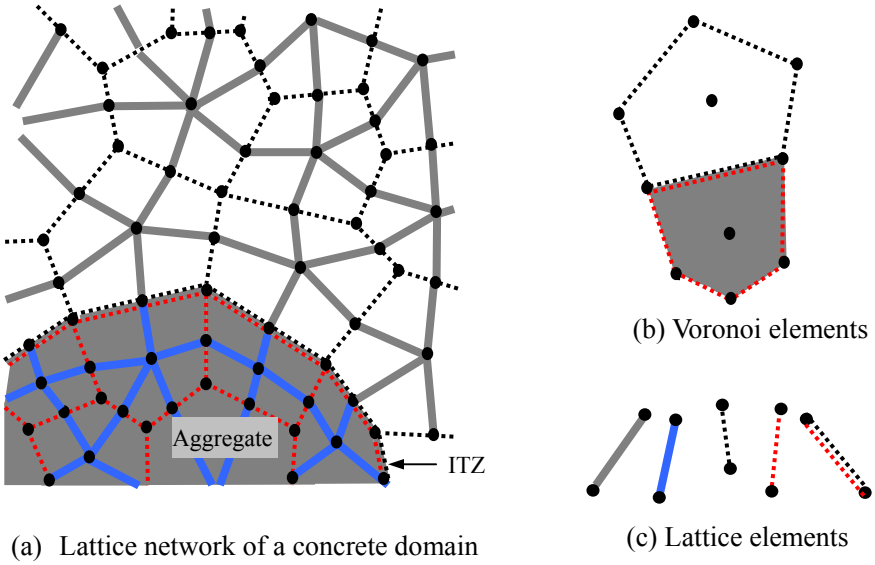

(a) Lattice network of a concrete domain

Fig. 4. Demonstration of the construction of the lattice network model

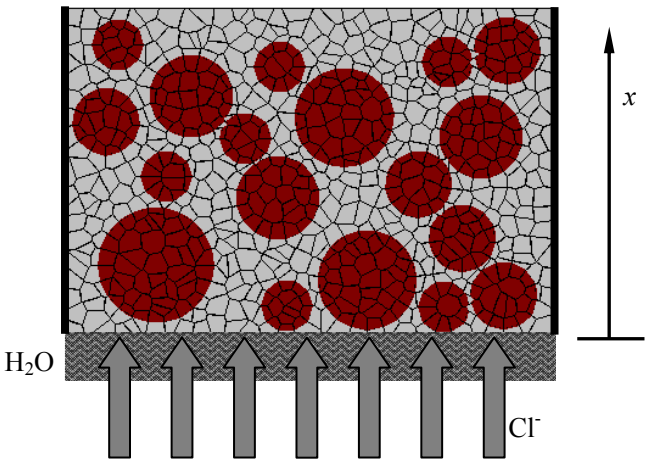

Fig. 5. Specimen model (width×height=50mm×60mm)

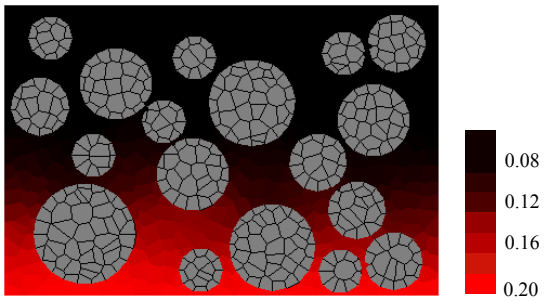

Fig. 7. Distribution of chloride (wt% of concrete) over the section of the specimen after 24 hrs

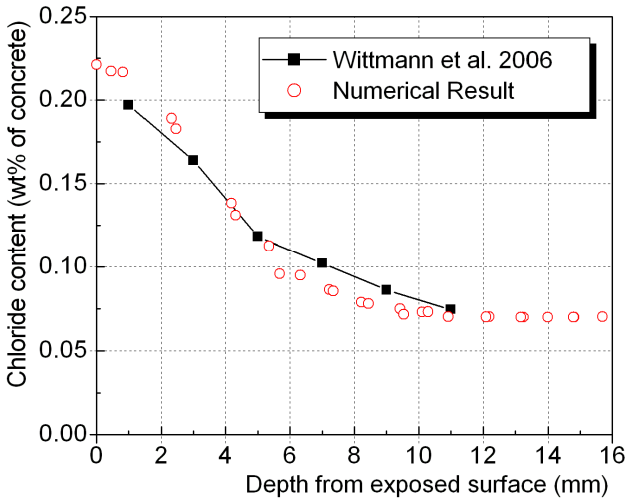

Fig. 8. Comparison of chloride profiles between test data and numerical result

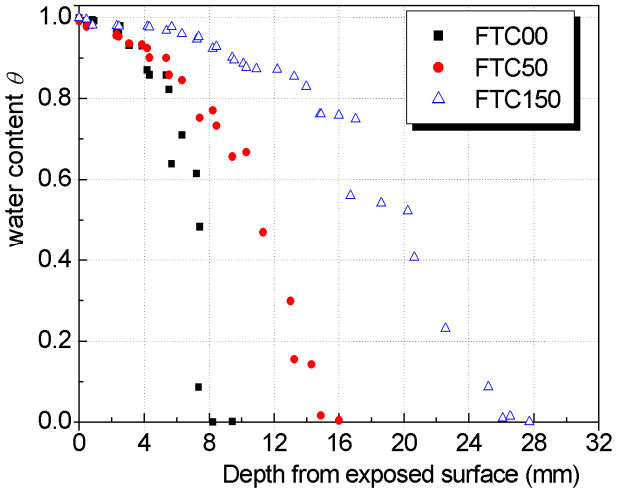

(a) Exposed time =8 hrs

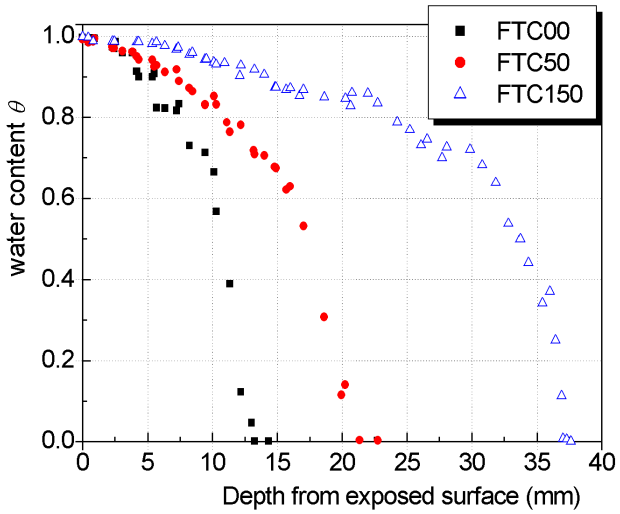

(b) Exposed time = 24 hrs

Fig. 9. Distribution of water content in concrete after subjected to 0, 50 and 150 FTCs

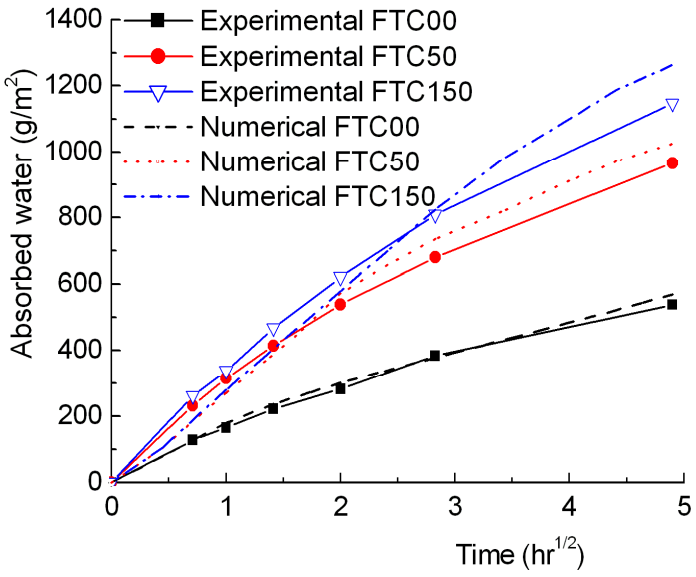

Fig. 10. Amount of water absorbed by the concrete after subjected to 0, 50 and 150 FTCs

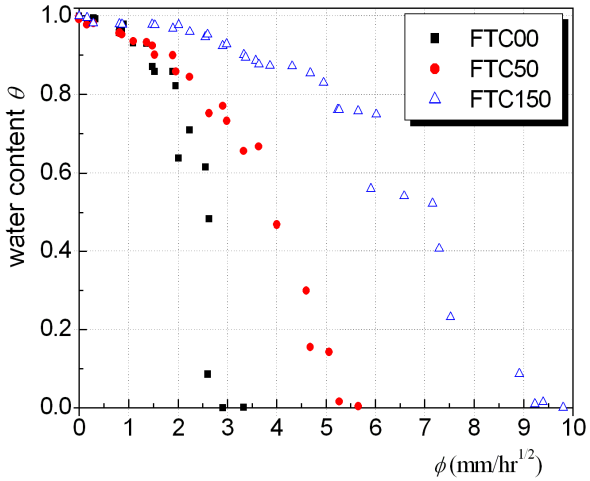

(a) Exposed time =8 hrs

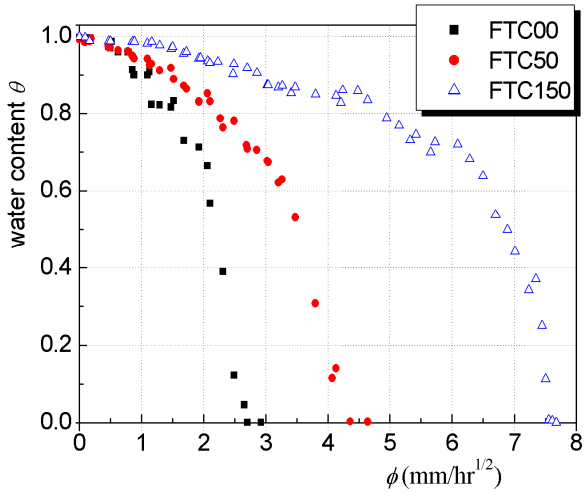

(b) Exposed time = 24 hrs

Fig. 11. Relationship between water content θ and Boltzmann variable ϕ

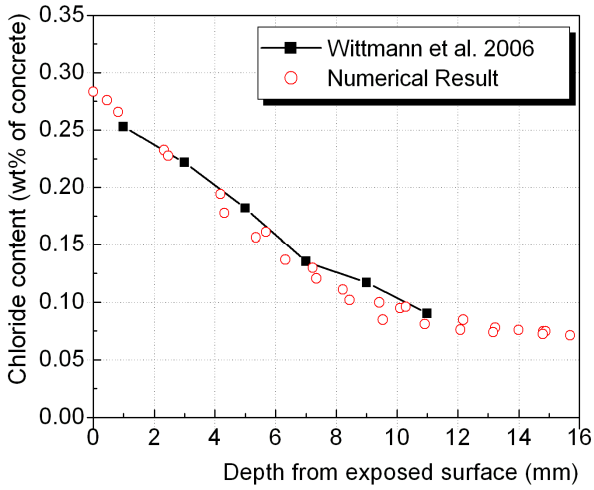

(a) 50 FTCs

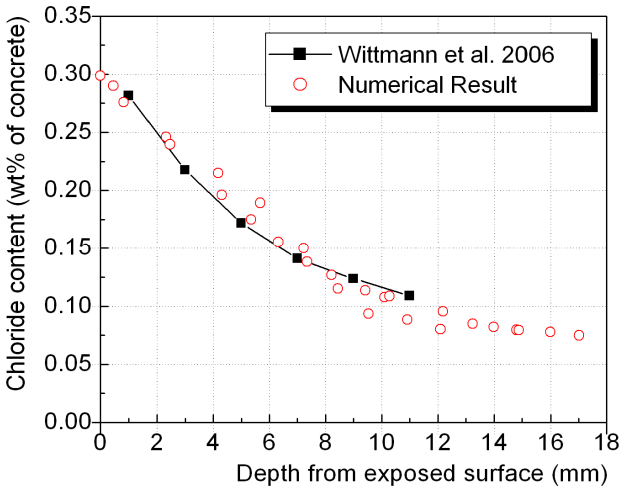

(b) 150 FTCs

Fig. 12. Comparison of chloride profiles after subjected to 50 and 150 FTCs

Table 1 Literatures summary on the D_{ITZ}

Series	Thickness of ITZ(μm)	D_{ITZ}/D_p	Reference
1	20-40	1.6-1.3	Yang 2003
2	30	16.2	Caré and Herve 2004
3	10-30	5	Delagrave et al. 1997
4	20	4-8	Oh and Jang 2004
5	-	6-12	Breton et al. 1992
6	20	2-6	Bentz et al. 1997
7	15-30	2-7	Shane et al. 2000

Table 2 Comparison of the strain and crack width from different tests

Ref.	Index	Number of FTCs		
		31	61	95
Jacobsen et al. 1996	$\Delta V/V_0$ (vol-%)	0.7	1.7	2.9
	ε ($\times 10^{-6}$)*	2328	5635	9575
	w_{cr} (μm)	5	9	12
Ref.	Index	Number of FTCs		
		50	100	150
Hasan et al. 2004	$\Delta V/V_0$ (vol-%)*	0.09	0.18	0.24
	ε ($\times 10^{-6}$)	314	596	809

* indicates the calculated results using the corresponding experimental data.

Table 3 Parameters for mass (water and chloride) transport in different phases of concrete

Diffusivity coefficient	Mortar	ITZ	Crack	Aggregate
D_0 (mm^2/hr)	0.06	0.541	4200	0
D_{cl1}(mm^2/hr)	0.35	3.5	3000	0